e-ISSN : 2987-0836 DOI: https://doi.org/10.59585/ijhs

Publish : Association of Indonesian Teachers and Lecturers
International Journal of Health Sciences (IJHS)
Journal Homepage : https://jurnal.agdosi.com/index.php/IJHS/index
Volume 4 | Number 4 | December 2026 |

Graphene Oxide/Fe_3O_4 Composites for Electromagnetic Wave Absorption in Radar Absorbing Material (RAM) Applications: A Critical Review of Design Principles, Loss Mechanisms and Performance

Ayyash Khoyyir Ahmad Kemal*, Sovian Aritonang, Hotma Renta,Muhammad Hafidh Husna, Afriza Rizky Putra Adjie, Muhammad Rizky Dayrobby

*Department of Physics, Faculty of Mathematics and Military Natural Sciences, Universitas Pertahanan Republik Indonesia, Bogor, Indonesia

Abstract

Graphene oxide (GO) and reduced graphene oxide (rGO) decorated with magnetite (Fe_3O_4) are among the most studied dielectric–magnetic hybrids for microwave absorption, yet their value for radar absorbing materials (RAM) is rarely judged against RAM-specific demands. This review surveys the field from three angles: how the oxidation degree of GO tunes permittivity and impedance matching; how synthesis routes set the Fe_3O_4 size, loading and interface quality; and how the resulting loss mechanisms translate into reflection loss (RL), effective absorption bandwidth (EAB) and matching thickness. Across roughly twenty representative studies, the best GO/rGO–Fe_3O_4 systems reach RL_{min} between about −43 and −66 dB at 2–3 mm, with EAB of 6–7 GHz in the Ku-band at low filler loadings (8–10 wt%) when a porous or hierarchical structure is used. Performance is strongly ratio-dependent, and a counter-example shows that pure Fe_3O_4 can outperform a poorly structured Fe_3O_4/rGO hybrid. Most work uses rGO rather than GO, so the benefit of retaining oxygen functional groups remains under-explored. We also discuss the unresolved debate on how RL and impedance matching should be interpreted, the weak comparability of paraffin-based coupon data, and the thin evidence for coating-scale, free-space or radar cross section (RCS) validation. A characterisation checklist for the graphene component, a reporting checklist and research priorities toward RAM-ready GO/Fe_3O_4 absorbers are proposed.

Keywords: Graphene Oxide, Fe_3O_4, Microwave Absorption, Radar Absorbing Material, Reflection Loss

Correspondent Author : Ayyash Khoyyir Ahmad Kemal
E-mail : kemalayyash@gmail.com

International Journal of Health Sciences is licensed under a Creative Commons Attribution 4.0 International License

e-ISSN : 2987-0836 DOI: https://doi.org/10.59585/ijhs

Publish : Association of Indonesian Teachers and Lecturers
International Journal of Health Sciences (IJHS)
Journal Homepage : https://jurnal.agdosi.com/index.php/IJHS/index
Volume 4 | Number 4 | December 2026 |

1. Introduction

Radar absorbing materials convert incident radar energy into heat and are a core passive countermeasure in military stealth, where they complement platform shaping to lower the radar cross section (RCS) (Kim et al., 2023). The same class of materials also addresses electromagnetic (EM) pollution from wireless and electronic devices, which is why microwave absorbers now serve both defense and civilian markets (Meng et al., 2018). An ideal absorber is expected to be thin, light, broadband and strongly absorbing, but these goals conflict: strong attenuation usually needs high conductivity, while high conductivity reflects the wave at the surface (Qin et al., 2022).

Carbon materials such as carbon black, fibres, nanotubes and graphene are attractive because of their low density, and they have been studied extensively as RAM fillers (Ruiz-Perez et al., 2022). Ferrites provide the permeability that carbon cannot supply, but they are heavy and limited by Snoek's law (Houbi et al., 2021). Combining the two is therefore a natural strategy, and graphene-based magnetic hybrids are widely regarded as a promising route to lightweight, high-performance absorbers (Peng et al., 2022). Early reports include reduced GO (Wen et al., 2014). Laminated magnetic graphene is another early example (Sun et al., 2013). Graphene-coated Fe has also been reported (Zhao et al., 2013). Graphene composites in general are reviewed in Stankovich et al. (2006).

GO is a useful carbon partner for a specific reason: its oxygen-containing groups and defects can anchor metal-ion nucleation, act as dipoles, and keep conductivity low enough to avoid severe impedance mismatch. Fully reduced graphene, in contrast, tends to have a permittivity that is too high, which restricts how much of the wave enters the absorber (Du et al., 2020). Fe_3O_4 is the usual magnetic partner because it is inexpensive and strongly magnetic, although its relatively small permittivity limits its use as a stand-alone absorber (Fu et al., 2018).

Graphene-based absorbers in general have been reviewed several times (Li et al., 2017). Carbon-based RAM has its own critical review (Ruiz-Perez et al., 2022). Ferrite composites have been reviewed separately (Houbi et al., 2021). Dielectric loss mechanisms are the subject of a dedicated review (Qin et al., 2022). Multi-interface heterostructures have also been reviewed (Cheng et al., 2021). The chemistry, synthesis and characterisation of GO itself are covered by reviews that do not discuss microwave absorption (Trikkaliotis et al., 2021).

2. Research Methods

This review is based on a web-based literature search carried out in November 2026 using terms combining graphene oxide, reduced graphene oxide, Fe_3O_4, microwave absorption, radar absorbing material, reflection loss, impedance matching and radar cross section. Sources were retained if they report measured EM parameters or RL for GO/rGO–Fe_3O_4 systems, or provide the theory and RAM background needed to interpret them.

3. Results and Discussion

RAM performance is judged in the radar bands that matter for the platform. Most laboratory studies measure 2–18 GHz, covering the S, C, X (8–12 GHz) and Ku (12–18 GHz) bands, and the X and Ku bands are the usual targets for fire-control and surveillance radar (Ruiz-Perez et al., 2022). The first RAM generation, developed during World War II, used ferrite and carbon-loaded composites and was thick and narrowband (Edries et al., n.d.). Stealth designs today combine shaping with RAM to minimise reflection toward the radar, and multilayer structures have been proposed to extend bandwidth (Ahmad et al., 2019). The radar-absorbing-structure literature also includes carbon-black glass/epoxy designs for the X-band (Oh et al., 2004). Surface geometry is also a lever: corrugated cavity structures have been reported to reach about −19.5 dB over 2.31–18 GHz regardless of wall material (Nurhasmi, 2026).

International Journal of Health Sciences is licensed under a Creative Commons Attribution 4.0 International License

e-ISSN : 2987-0836 DOI: https://doi.org/10.59585/ijhs

Publish : Association of Indonesian Teachers and Lecturers
International Journal of Health Sciences (IJHS)
Journal Homepage : https://jurnal.agdosi.com/index.php/IJHS/index
Volume 4 | Number 4 | December 2026 |

Absorbers can be grouped as impedance-matching types and resonant types, and the materials themselves are resistive, magnetic or both (Saville, 2005). Table 1 summarises how the main classes relate to the GO/Fe_3O_4 design logic.

Table 1. Classes of microwave absorbers and how they relate to the GO/Fe_3O_4 design logic.

Absorber class	Typical materials	Main strength	Main limitation	Source
Carbon dielectric	Carbon black, fibres, CNT, graphene, rGO	Low density, high dielectric loss	Impedance mismatch when too conductive; agglomeration	Ruiz-Perez et al., 2022
Ferrite magnetic	Spinel ferrites, hexaferrites	Magnetic loss, thermal and chemical stability	High density, Snoek limit, narrow band	Houbi et al., 2021
Metallic magnetic	Carbonyl iron, Fe, Co, alloys	High saturation magnetization	Eddy currents, oxidation, weight	Du et al., 2020
Carbon/ferrite hybrid	GO or rGO with Fe_3O_4 and other ferrites	Dielectric–magnetic synergy, tunable matching	Ratio and structure sensitive; scale-up	Peng et al., 2022
Structural/geometric	Multilayers, corrugated or cavity surfaces	Bandwidth independent of composition	Thickness, manufacturing complexity	Nurhasmi, 2026

For RAM, three practical constraints go beyond the RL curves reported in most papers: the areal density at the matching thickness, the ability to sit in a coating or structural laminate rather than a paraffin ring, and stability in the service environment. Section 3.8 returns to these constraints.

Most absorber papers model a single layer backed by a perfect conductor and use transmission-line theory (Naito & Suetake, 1971). In this model, the input impedance of the layer depends on the complex relative permittivity and permeability of the material, on its thickness and on the frequency of the wave. Reflection loss (RL), expressed in decibels, compares that input impedance with the impedance of free space (about 377 Ω): the closer the two are, the weaker the reflected wave and the more negative the RL. An RL of −10 dB corresponds to 90% absorption and −20 dB to 99%. The effective absorption bandwidth (EAB) is the frequency span over which RL stays at or below −10 dB.

Permittivity and permeability each have a real part, which describes energy storage, and an imaginary part, which describes energy loss (Zhang et al., 2021). Two conditions are usually named for good absorption: impedance matching, so that the wave enters the absorber, and attenuation capacity, so that the wave is dissipated inside it (Zhang et al., 2021). Perfect matching would need equal relative permittivity and permeability, which is hard to achieve, so both are adjusted artificially through composition and structure (Zhang et al., 2021).

The thickness at which an absorption peak appears is often compared with the quarter-wavelength model. It states that the peak occurs when the layer thickness equals an odd multiple of a quarter of the wavelength inside the material, so thicker layers move the peak to lower frequency, and a higher product of permittivity and permeability moves it to a smaller thickness. The attenuation constant, calculated from the real and imaginary parts of both permittivity and permeability, describes the intrinsic ability of the material to dissipate the wave. Table 2 (Section 3.2.4) summarises these quantities. Section 3.9 discusses a growing body of critique arguing that these tools are often applied outside their valid range (Y. Liu, Drew, et al., 2023).

International Journal of Health Sciences is licensed under a Creative Commons Attribution 4.0 International License

e-ISSN : 2987-0836 DOI: https://doi.org/10.59585/ijhs

Publish : Association of Indonesian Teachers and Lecturers
International Journal of Health Sciences (IJHS)
Journal Homepage : https://jurnal.agdosi.com/index.php/IJHS/index
Volume 4 | Number 4 | December 2026 |

At GHz frequencies, dielectric loss is dominated by conduction loss, interfacial polarization, dipolar polarization and defect-induced polarization, whereas ionic and electronic polarization lie at much higher frequencies and are seldom relevant (Qin et al., 2022). The imaginary permittivity can therefore be separated into a polarization part, which follows Debye relaxation, and a conduction part, which grows with electrical conductivity and falls with frequency.

Each Debye relaxation process appears as a semicircle in the Cole–Cole plot of imaginary against real permittivity, while a straight tail indicates conduction loss (Quan et al., 2017). A recurring problem in the literature is that interfacial, dipole and defect polarization are used interchangeably and their contributions are asserted rather than quantified (Qin et al., 2022).

Magnetic loss in the GHz range comes from natural resonance, exchange resonance and eddy currents (Zhou et al., 2026). Natural resonance is tied to the anisotropy field, and the ceiling on permeability at a given frequency is set by Snoek's law (Snoek, 1948). Some reviews attribute resonance peaks in 2–8 GHz to exchange resonance and those above 8 GHz to natural resonance (Zhou et al., 2026), although the assignment should be backed by measurements and not by frequency alone. Eddy-current loss is tested with a coefficient built from the imaginary permeability, the square of the real permeability and the frequency. If this coefficient stays constant with frequency, eddy currents dominate; if it fluctuates, resonance contributes (Zhou et al., 2026). In metallic magnetic nanoparticles with high conductivity, eddy currents can also reduce the effective magnetization (Du et al., 2020).

Table 2. Quantities used to evaluate microwave absorbers and how GO/Fe_3O_4 studies use them.

Quantity	What it tells the reader	Common use in GO/Fe_3O_4 papers
Reflection loss (RL)	Strength of absorption at a given thickness and frequency	Headline value (RL_{min}) and RL maps against thickness
Effective absorption bandwidth (EAB)	Frequency span with at least 90% absorption	Bandwidth at the best thickness
Impedance matching	How much of the wave enters the layer	Map of normalized input impedance against frequency and thickness
Attenuation constant	Intrinsic ability to dissipate the wave	Compared across filler ratios
Cole–Cole plot	Number of dielectric relaxation processes	Evidence for interfacial and dipolar relaxation
Eddy-current coefficient	Whether eddy currents or resonance dominate magnetic loss	Frequency plot of the coefficient
Quarter-wavelength model	Whether peak position agrees with interference at a quarter wavelength	Check of measured thickness against predicted thickness

Graphene is a single layer of sp^2-bonded carbon about 0.335 nm thick, with a C–C bond length of about 0.142 nm; stacking such layers with weak van der Waals forces gives graphite (Figure 1) (Trikkaliotis et al., 2021). Oxidising graphite turns part of the planar sp^2 network into tetrahedral sp^3 carbon and attaches oxygen groups: epoxy and hydroxyl groups on the basal plane, and carboxyl and hydroxyl groups at the edges (Figure 2) (J. Liu et al., 2022). The C/O atomic ratio of GO is roughly 2–3, the interlayer spacing grows from 0.335 nm to about 0.9–1.3 nm, the conjugated network is broken, electrical conductivity falls sharply, and the sheet becomes hydrophilic (Trikkaliotis et al., 2021).

International Journal of Health Sciences is licensed under a Creative Commons Attribution 4.0 International License

e-ISSN : 2987-0836 DOI: https://doi.org/10.59585/ijhs

Publish : Association of Indonesian Teachers and Lecturers
International Journal of Health Sciences (IJHS)
Journal Homepage : https://jurnal.agdosi.com/index.php/IJHS/index
Volume 4 | Number 4 | December 2026 |

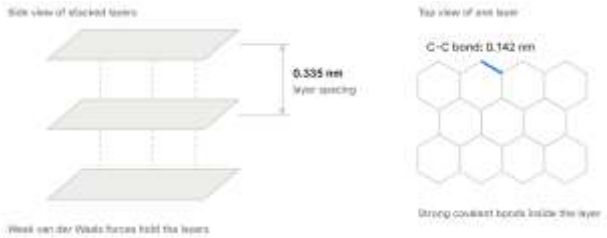


Figure 1. *Graphite structure: weak van der Waals forces hold the layers 0.335 nm apart, while each layer is a honeycomb of C–C bonds 0.142 nm long. Original schematic drawn for this review after the structure described in Trikkaliotis et al. (2021).*



Figure 2. Typical structures of (a) graphene and (b) GO, with hydroxyl and epoxy groups on the basal plane and carboxyl groups at the edges. Original schematic drawn for this review after the structures described in Liu et al. (2022).

GO is non-stoichiometric and polydisperse, so its exact structure is still debated (J. Liu et al., 2022). Three models are used. The Lerf–Klinowski model, built on NMR data, describes sp^2 islands inside an oxidised matrix of epoxy and hydroxyl groups, with carboxyl groups at edges and holes (Lerf et al., 1998). It remains the most widely accepted model (Trikkaliotis et al., 2021). It cannot explain the strong acidity of GO, which the dynamic structural model of Dimiev, Alemany, and Tour (2013) attributes to enol-type acid structures and residual covalent sulfate formed as GO reacts with water. In that view the structure keeps changing during washing and storage. GO solutions typically have a pH of 2.0–4.5 (Trikkaliotis et al., 2021). The two-component model of Rourke et al. (2011) proposes that GO consists of intact, less oxidised sheets plus small fragments called oxidation debris, which can make up about one third of the mass and are removed by base washing.

Three consequences matter for absorbers. First, the oxygen groups and their distribution are the origin of the dipolar and defect polarization sites, and of the Fe-ion anchoring sites, invoked in Section 3.5. Second, GO is metastable: it has been reported to release CO_2 at temperatures as low as 45 °C, and its mass loss proceeds in stages up to about 260 °C, with adsorbed water leaving up to roughly 160 °C and labile groups and bound water after that (Trikkaliotis et al., 2021). Fe_3O_4 co-precipitation near 80 °C and hydrothermal or solvothermal growth at 100–180 °C (Section 3.4) can therefore be expected to modify the carbon even when the starting material is GO, which should be confirmed by XPS. Third, the oxidation degree can differ between flakes of the same batch, and the sp^2 domains grow with storage time (Trikkaliotis et al., 2021), which may be a hidden source of batch-to-batch scatter in permittivity.

International Journal of Health Sciences is licensed under a Creative Commons Attribution 4.0 International License

e-ISSN : 2987-0836 DOI: https://doi.org/10.59585/ijhs

Publish : Association of Indonesian Teachers and Lecturers
International Journal of Health Sciences (IJHS)
Journal Homepage : https://jurnal.agdosi.com/index.php/IJHS/index
Volume 4 | Number 4 | December 2026 |

Table 3. Main routes to graphene oxide.

Route	Oxidant system	Main advantage	Main limitation	Source
Brodie (1859)	$KClO_3$ in fuming HNO_3	First GO route	Explosion risk, days of reaction, toxic gas	J. Liu et al., 2022
Staudenmaier (1898)	$KClO_3$ in H_2SO_4/HNO_3	Safer and more efficient than Brodie	About 4 days at high temperature; chlorate not fully abandoned	J. Liu et al., 2022
Hummers–Offeman (1958)	$KMnO_4$ and $NaNO_3$ in H_2SO_4	In-situ nitric acid, high oxidation	NO_x gas, Mn and Na^+/NO_3^- residues, explosive Mn_2O_7 at elevated temperature	Hummers & Offeman, 1958
Improved Hummers (2010)	$KMnO_4$ in H_2SO_4/H_3PO_4 (9:1), no $NaNO_3$	Higher efficiency, no toxic gas, easier temperature control; common for scale-up	Large permanganate use	Marcano et al., 2010
Iron-based (2015)	K_2FeO_4 in H_2SO_4	Room temperature, about 1 h, no heavy-metal ions or explosion risk	Newer, little used in absorber studies	Peng et al., 2015
Bottom-up, Tang–Lau (2012)	Glucose, sucrose or fructose; hydrothermal growth then annealing	Eco-friendly; thickness controllable; monolayer lateral size 1 nm–1500 nm	None found in absorber studies in this survey	Tang et al., 2012
Electrochemical exfoliation	Graphite rods in H_2SO_4 under DC bias	Non-toxic	Product is closer to graphene than GO	J. Liu et al., 2022

Table 3 lists the main routes. All top-down routes follow three stages: intercalation, oxidation and exfoliation. In the Hummers method, $KMnO_4$ reacts with cold concentrated H_2SO_4 to give the active oxidant Mn_2O_7, sulfuric acid intercalates first, oxidation follows, and water and H_2O_2 then hydrolyse and exfoliate the graphite oxide (Dimiev & Tour, 2014). The oxidant therefore sets the oxygen content, the defects and the amount of debris (J. Liu et al., 2022). Over-oxidation, indicated by a C/O ratio below about 2.5 (carbon content below 55%), breaks the lattice and releases CO_2, and pre-oxidation before the Hummers step raises the oxidation rate (Trikkaliotis et al., 2021). Drying also matters: freeze-drying avoids potassium-related flammability but can promote partial restacking, and spray-drying is an alternative (Trikkaliotis et al., 2021).



Figure 3. Bottom-up Tang–Lau route to GO nanosheets (GON): glucose polymerisation, transfer, cleaning and annealing. Original schematic drawn for this review after the route described in Tang et al. (2012).

For absorber work the practical point is that the starting permittivity is set by the route, the washing and the drying protocol. A study should therefore state the route, the oxidant ratio, the purification and drying steps, and the measured C/O ratio of the GO it started from.

International Journal of Health Sciences is licensed under a Creative Commons Attribution 4.0 International License

e-ISSN : 2987-0836 DOI: https://doi.org/10.59585/ijhs

Publish : Association of Indonesian Teachers and Lecturers
International Journal of Health Sciences (IJHS)
Journal Homepage : https://jurnal.agdosi.com/index.php/IJHS/index
Volume 4 | Number 4 | December 2026 |

Table 4. Characterisation checklist for the oxidation state of GO.

Technique	Typical signature of GO	What it tells the absorber designer	Source
XRD	(001) peak near 2θ ≈ 10° (graphite near 26°); sometimes a weak peak near 43°	Oxidation and exfoliation; whether the GO peak survives Fe_3O_4 growth	Trikkaliotis et al., 2021
FTIR	≈3400 cm^{-1} O–H; ≈1730 cm^{-1} C=O; 1590–1620 cm^{-1} C=C; ≈1050 cm^{-1} C–O (epoxy/alkoxy)	Inventory of oxygen groups; adsorbed water (up to about 25% of mass) complicates the spectrum	Trikkaliotis et al., 2021
Raman	D ≈1350, G ≈1580 and 2D ≈2680 cm^{-1}; I_D/I_G near 0.95 for GO, usually rising after chemical reduction	Defect density; the rise after reduction reflects smaller sp^2 domains	J. Liu et al., 2022
XPS	C 1s: C–C 284.4 eV, C–O 285.3 eV, C=O 288.0 eV; O 1s sub-peaks	C/O ratio and group fractions; more reliable for oxygen than elemental analysis	J. Liu et al., 2022
TGA	Mass loss at 100–160 °C (adsorbed water), 160–260 °C (bound water, labile groups to CO_2), then above 260 °C	Oxidation state of the carbon; carbon burn-off against Fe_3O_4 fraction in the composite	J. Liu et al., 2022
UV–Vis	π→π* peak near 230 nm; n→π* shoulder near 300 nm; the shoulder fades and visible absorption rises on reduction	Quick check of reduction in dispersion (Figure 4)	Trikkaliotis et al., 2021
AFM / TEM	GO monolayer about 1 nm thick (graphene 0.34 nm)	Exfoliation state and lateral size	J. Liu et al., 2022
N_2 porosimetry	Specific surface area: graphite about 6, GO about 50, graphene about 2600 m^2 g^{-1}	Porosity of hierarchical or aerogel composites	Trikkaliotis et al., 2021

Table 4 lists the signatures to check. Trikkaliotis et al. (2021) suggest running XRD first, followed by FTIR and AFM, with Raman and XPS being essential for rGO. The same set, applied to both the starting GO and the final composite, would make the carbon state of a GO/Fe_3O_4 absorber verifiable.

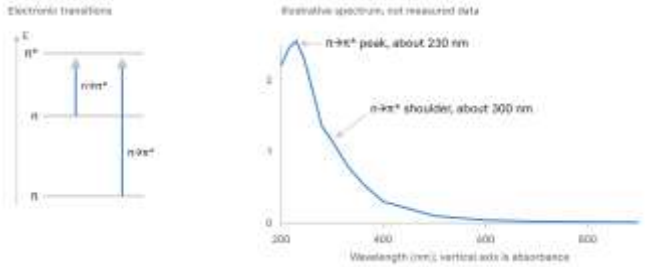


Figure 4. Electronic transitions in GO (left) and an illustrative UV–Vis spectrum with a π→π* peak near 230 nm and an n→π* shoulder near 300 nm (right). The curve is a sketch, not measured data; original schematic drawn for this review after the features described in Trikkaliotis et al. (2021).

GO is an electrical insulator, with a sheet resistance of the order of 10^{12} Ω per square and a conductivity of about 10^{-3} S m^{-1}, because its oxygen groups isolate the sp^2 areas (Trikkaliotis et al., 2021). Reduction removes oxygen and restores the conjugated network, so the C/O ratio

International Journal of Health Sciences is licensed under a Creative Commons Attribution 4.0 International License

e-ISSN : 2987-0836 DOI: https://doi.org/10.59585/ijhs

Publish : Association of Indonesian Teachers and Lecturers
International Journal of Health Sciences (IJHS)
Journal Homepage : https://jurnal.agdosi.com/index.php/IJHS/index
Volume 4 | Number 4 | December 2026 |

is the main design parameter for the permittivity of the carbon phase. C/O is about 2–3 for GO and 4–12 for rGO, and a value near 10 indicates good conductivity when the lattice is intact (Trikkaliotis et al., 2021). The ratio can be tuned through the reduction conditions (Compton et al., 2011). The temperature windows are well documented: most functional groups are lost between 160 and 300 °C, carbonyls survive up to about 500 °C, the sp^2 network reconstructs above 700 °C, and more than 900 °C is needed to reach less than 1% oxygen; annealing near 900 °C gives rGO conductivities of 200–300 S cm^{-1} (Trikkaliotis et al., 2021). Solvothermal deoxygenation in NaOH or KOH is possible below 100 °C, and chemical reductants include hydrazine, $NaBH_4$ and HI with acetic acid, as well as milder ascorbic acid, alanine and glucose (Pei & Cheng, 2012). Because these ranges overlap with the conditions used to grow Fe_3O_4 (Section 3.4), reduction is usually a side effect of the synthesis and not a controlled step.

Three studies make this concrete. In a hydrothermal series, raising the reaction temperature from 100 to 180 °C increased the C/O atomic ratio of rGO from 6.35 to 9.44 and gave tunable permittivity and improved absorption, with the authors noting that well-reduced rGO tends to mismatch impedance with air (Xia et al., 2018). Annealing temperature has been shown to affect permittivity and attenuation in the same way (Wu et al., 2018b). A separate study found that partial reduction of GO strengthens its response to microwaves, with lower-oxidation GO deoxygenating more efficiently (Gu et al., 2019). Taken together, these reports indicate that an intermediate oxidation state, not full reduction, may offer the best match when a magnetic phase supplies the permeability. Most Fe_3O_4 hybrids in the literature are nevertheless made by processes that reduce GO in situ (Section 3.4), so the oxidation state of the final carbon is often unreported.

Pristine graphene and heavily reduced rGO are limited by high permittivity and low permeability, which gives poor impedance matching and weak absorption on their own (Du et al., 2020). Agglomeration and restacking of rGO sheets further degrade matching (Fu et al., 2018).

These data suggest a design rule, which is a proposal and not an established result: the best permittivity is likely to lie between insulating GO (C/O about 2–3) and well-reduced rGO (C/O near 10). A series of GO/Fe_3O_4 composites at fixed Fe_3O_4 content, prepared with the carbon at several C/O values across that range and characterised as in Section 3.3.3, would test this directly.

Fe_3O_4 is an inverse-spinel ferrimagnet with a bulk saturation magnetization of roughly 90 emu g^{-1} and electron hopping between Fe^{2+} and Fe^{3+} sites that gives moderate conductivity. As a stand-alone absorber it offers magnetic loss but relatively low permittivity (Fu et al., 2018). Its natural resonance is bounded by Snoek's law (Snoek, 1948). Its size and morphology matter: flower-like, hollow, nanorod, nanotube and porous forms have all been reported to change EM parameters and absorption (Adebayo et al., 2020). Because Fe_3O_4 nanoparticles agglomerate magnetically, a graphene support that spaces them apart is a second benefit of the hybrid (Fu et al., 2018)

The combination attacks both halves of the absorber problem: Fe_3O_4 lowers the effective ε/μ contrast and adds magnetic loss, while GO/rGO adds dielectric loss, polarization sites and a light, high-surface-area support (Peng et al., 2022). It does not always work. In solution-combustion powders, pure Fe_3O_4 reached −33 dB with a 3 GHz bandwidth at 1.2 mm, whereas the Fe_3O_4/rGO powder made with urea fuel reached −28 dB with only 1.4 GHz at 3.7 mm; the authors attribute the difference to impedance matching helped by the porous microstructure of the pure Fe_3O_4 powder (Tayebi Pak et al., 2021). The lesson is that adding graphene is not sufficient; the carbon content, structure and interface must be tuned.

Synthesis decides four things that the EM data later reflect: the Fe_3O_4 phase purity and size, the oxidation state of the carbon, the quality of the Fe_3O_4–carbon interface, and the macroscopic architecture. The routes in the literature fall into the groups in Table 5.

International Journal of Health Sciences is licensed under a Creative Commons Attribution 4.0 International License

e-ISSN : 2987-0836 DOI: https://doi.org/10.59585/ijhs

Publish : Association of Indonesian Teachers and Lecturers
International Journal of Health Sciences (IJHS)
Journal Homepage : https://jurnal.agdosi.com/index.php/IJHS/index
Volume 4 | Number 4 | December 2026 |

Table 5. Synthesis routes for GO/rGO–Fe_3O_4 composites.

Route	Typical conditions and outcome	Strength	Limitation	Source
Co-precipitation	Fe^{3+}/Fe^{2+} with base in a GO dispersion, mild temperature	Scalable, mild conditions; carbon is usually less reduced than in hydrothermal routes (confirm by XPS)	Broad size distribution; phase impurities	Massart, 1981
One-pot hydrothermal / solvothermal	GO reduced while Fe_3O_4 grows; ethylene glycol or water	Good dispersion; morphology control; about 15 nm particles reported	GO is usually reduced to rGO; autoclave scale	Du et al., 2020
One-pot GO decoration	Fe_3O_4 grown on GO, GO:Fe_3O_4 ratio tuned	Simple, scalable; ratio tunes dielectric–magnetic balance	Oxidation state of GO needs confirmation	Huang et al., 2026
Thermochemical	Graphite oxide with $FeSO_4 \cdot 7H_2O$ at 500–800 °C; α-Fe_2O_3 → γ-Fe_2O_3 → Fe_3O_4 regulated by rGO	Phase control by temperature; stable to 800 °C	High temperature; fully reduced carbon	Zhang et al., 2015
Solution combustion	Fuel type (glycine or urea) sets phase and porosity	Fast; porous powders	Phase mixtures (α-Fe_2O_3/Fe_3O_4) with urea	Tayebi Pak et al., 2021
Covalent grafting	Amide bonds between rGO and Fe_3O_4	Strong interface; reported RCS simulation	Multi-step	Liu et al., 2021
Template or CVD plus hydrothermal	Graphene capsules with Fe_3O_4 on inner and outer walls	Unique sandwich morphology	Complex, costly	Jian et al., 2016
3D assembly	Freeze-drying and thermal treatment to aerogels or porous networks	Low filler loading (8 wt%); suppressed restacking	Mechanical weakness; processing	Shi et al., 2026
Film or buckypaper	Fe_3O_4/GO sheets laminated onto composites	Flexible; integrates with fibre composites	Thickness control; filler content	Wang et al., 2019

Three observations follow. First, hydrothermal and thermal routes are the most popular but they convert GO to rGO, so the "GO/Fe_3O_4" label in many titles describes the starting material and not the final carbon. Second, rGO also helps phase formation: it has been shown to steer the α-Fe_2O_3 to γ-Fe_2O_3 to Fe_3O_4 transformation, and the oxygen groups and hydrogen released during annealing are thought to play a role (Zhang et al., 2015). Third, small changes to the carbon fraction alter Fe_3O_4 morphology: in one solvothermal study, raising the rGO content shifted Fe_3O_4 from self-assembled solid or flower-like structures to monodisperse nanoparticles, and a GO content of 10 wt% gave the best matching (Ren et al., 2021). Likewise, the concentration of GO changed Fe_3O_4/graphene from flower-like to solid spheres in another report (Zhang et al., 2016).

For a future GO-retaining design, the minimum characterisation set is the checklist of Section 3.3.3 (XRD, FTIR, Raman, XPS, TGA and UV–Vis), applied to both the starting GO and the final composite (Trikkaliotis et al., 2021).

The studies reviewed here explain absorption through the same set of mechanisms. Their relative weight depends on composition and structure, and it is rarely measured directly.

International Journal of Health Sciences is licensed under a Creative Commons Attribution 4.0 International License

e-ISSN : 2987-0836 DOI: https://doi.org/10.59585/ijhs

Publish : Association of Indonesian Teachers and Lecturers
International Journal of Health Sciences (IJHS)
Journal Homepage : https://jurnal.agdosi.com/index.php/IJHS/index
Volume 4 | Number 4 | December 2026 |

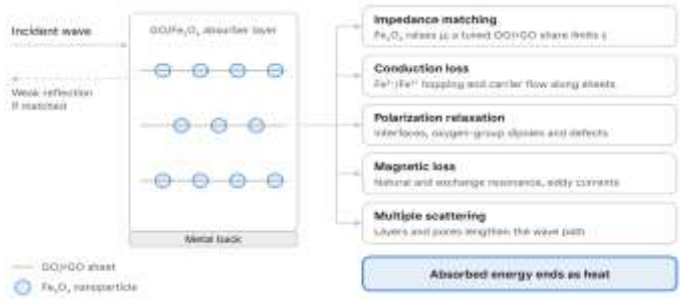


Figure 5. Mechanism schematic. Fe_3O_4 and the GO/rGO sheets act through five channels at once; their relative weights depend on composition and structure and should be shown with measurements, not assumed.

Impedance matching. Adding Fe_3O_4 raises permeability and, together with a limited graphene fraction, brings the effective impedance closer to that of free space. The reported optimum is a narrow window of graphene content, for example GO at 10 wt% in one series (Ren et al., 2021). Heat-reduced hybrids with epoxy used a small rGO fraction: rGO alone gave only −10 dB at 2 mm, but the Fe_3O_4 hybrid reached −22.2 dB at 17.3 GHz (H.-K. Liu et al., 2023). The effect of GO loading on Fe_3O_4/rGO hybrids has been examined directly (Wu et al., 2017). Varying the GO:Fe_3O_4 ratio is the main tuning knob in GO-based one-pot materials (Huang et al., 2026).

Conduction loss. Electron migration along carbon sheets and hopping between Fe^{2+} and Fe^{3+} convert EM energy to heat. It increases attenuation but, if the percolated network is too conductive, it worsens the matching (Qin et al., 2022).

Polarization relaxation. Three polarization sources coexist: interfacial polarization at the Fe_3O_4/carbon boundary and at the filler/matrix boundary; dipolar polarization at oxygen-containing groups; and defect-induced polarization at vacancies and lattice defects (Quan et al., 2017). Heterointerfaces are cited as the main reason a Fe_3O_4 flake/rGO composite outperformed pure Fe_3O_4 flakes and a granular Fe_3O_4/rGO composite, with RL of −47.2 dB at 2.4 mm (Jiao et al., 2020). Density functional theory work on Fe_3O_4/Fe@rGO shows pronounced charge transfer at the Fe_3O_4/Fe interface, giving atomistic support for interfacial loss (Pan et al., 2026). Critical reviews warn that these polarization terms are often confused and that the contribution of an interface is rarely quantified (Qin et al., 2022).

Magnetic loss. Natural and exchange resonance and eddy currents contribute to μ″. In Fe_3O_4/graphene-capsule composites, transmission-line simulation combined with eddy-current analysis was used to separate these contributions (Jian et al., 2016). The same caution as in Section 3.2 applies: a frequency-independent eddy-current coefficient supports eddy-current loss, but an assignment of peaks to exchange resonance purely from frequency position is weak evidence (Zhou et al., 2026).

Multiple scattering and path extension. Layered, porous or hollow architectures lengthen the wave path, and 3D graphene aerogels carrying Fe_3O_4 microflowers suppress restacking and promote multiple scattering, which is credited for −63.2 dB at 2.7 mm and 6.89 GHz EAB at only 8 wt% (Shi et al., 2026).

Synergy is a design target, not a given. The counter-example of Section 3.3.6 (Tayebi Pak et al., 2021) shows that adding rGO can reduce performance if the matching worsens. The most credible mechanistic papers therefore combine three measurements: Cole–Cole analysis for relaxation, the eddy-current coefficient against frequency, and an impedance-matching map against frequency and thickness, rather than listing mechanisms from the literature.

International Journal of Health Sciences is licensed under a Creative Commons Attribution 4.0 International License

e-ISSN : 2987-0836 DOI: https://doi.org/10.59585/ijhs

Publish : Association of Indonesian Teachers and Lecturers
International Journal of Health Sciences (IJHS)
Journal Homepage : https://jurnal.agdosi.com/index.php/IJHS/index
Volume 4 | Number 4 | December 2026 |

Table 6 collects representative values reported for GO/rGO–Fe_3O_4 systems and close relatives. "n/r" means not reported in the source consulted. The values come from different matrices, filler loadings and measurement set-ups, so they show trends, not a ranking.

Table 6. Representative absorption performance of GO/rGO–Fe_3O_4 systems and close relatives.

Material	Carbon state	RL_{min} (dB) and frequency or thickness	EAB (RL ≤ −10 dB)	Source
Fe_3O_4/graphene, flower-like	rGO/graphene	−53.2	8.1–16 GHz	Zhang et al., 2016
rGO-wrapped super-dense Fe_3O_4	rGO	−55.71 at 6.78 GHz, 3.5 mm	n/r	Yu et al., 2019
Fe_3O_4 nanoparticles on rGO (15.3 nm)	rGO	−34.4 at 1.6 mm; −37.5 at 6.5 mm	3.8 GHz; 1.9 GHz	Du et al., 2020
Fe_3O_4 flakes/rGO	rGO (H_2 reduced)	−47.2 at 2.4 mm	6.4 GHz (11.36–17.76)	Jiao et al., 2020
Fe_3O_4/rGO, 10 wt% GO	rGO	−64.7 at 6.6 GHz, 4.5 mm	13.6 GHz over 1.5–5 mm	Ren et al., 2021
Heat-reduced rGO/Fe_3O_4/epoxy	rGO	−22.2 at 17.3 GHz, 2 mm	n/r	H.-K. Liu et al., 2023
Fe_3O_4@PEDOT/rGO	rGO	−48.8 at 9.12 GHz, 2.9 mm	4.32 GHz	Chen et al., 2021
Fe_3O_4/$CoCO_3$@rGO, 25 wt%	rGO	−24.4 at 14.64 GHz, 2.3 mm; −32.4 at 13.68 GHz, 1.8 mm	6.24 GHz (11.76–18); 6.56 GHz at 2.1 mm	Li et al., 2024
Fe_3O_4/FeS_x hollow spheres/rGO aerogel	rGO	−43.03 at 2.0 mm	4.24 GHz at 1.6 mm	J. Zhang et al., 2024
3D RGO/Fe_3O_4 microflowers, 8 wt%	rGO aerogel	−63.2 at 2.7 mm	6.89 GHz	Shi et al., 2026
Fe_3O_4/Fe@rGO	rGO	−66.4 at 2.7 mm	7.16 GHz	Pan et al., 2026
rGO/Fe_3O_4 (1:2) in silicone, infrared stealth	rGO	−31.3 at 15.3 GHz, 2.0 mm	n/r	Wu et al., 2022
Fe_3O_4/rGO combustion powder (urea fuel)	rGO	−28 at 3.7 mm	1.4 GHz	Tayebi Pak et al., 2021
Pure Fe_3O_4 combustion powder (glycine fuel)	none	−33 at 1.2 mm	3 GHz (Ku)	Tayebi Pak et al., 2021
Fe_3O_4@GO, one-pot (ratio tuned)	GO	−58.37 at 8.28 GHz, 3.1 mm; RCS below −16.06 dB m² over −90° to 90°, minimum −29.04 dB m² at 10°	5.13 GHz (12.87–18) at 1.8 mm	Huang et al., 2026
Fe/RGO (non-Fe_3O_4 reference), 10 wt%	rGO	−67.95 at 8.48 GHz	6.91 GHz (11.09–18)	K. Zhang et al., 2024

Best-case performance is high but clusters in the Ku-band. Systems with a dedicated architecture (flakes, microflowers, Fe_3O_4/Fe heterojunctions, FeS_x hollow spheres) reach −43 to −66 dB at 2–3 mm, and several report 6–7 GHz of EAB between about 11 and 18 GHz (Table 6). Low-frequency (S/C-band) absorption from the same hybrids needs 3.5–6.5 mm, which is thick for RAM (Table 6).

The graphene fraction has an optimum. A GO content of 10 wt% gave the best matching in one solvothermal series (Ren et al., 2021). Heat-reduced rGO at sub-percent levels in an epoxy matrix was used to tune permittivity against Fe_3O_4 (H.-K. Liu et al., 2023). GO loading effects on Fe_3O_4/rGO are documented in Wu et al. (2017). The GO:Fe_3O_4 ratio is also the central variable in

International Journal of Health Sciences is licensed under a Creative Commons Attribution 4.0 International License

e-ISSN : 2987-0836 DOI: https://doi.org/10.59585/ijhs

Publish : Association of Indonesian Teachers and Lecturers
International Journal of Health Sciences (IJHS)
Journal Homepage : https://jurnal.agdosi.com/index.php/IJHS/index
Volume 4 | Number 4 | December 2026 |

the one-pot Fe_3O_4@GO work (Huang et al., 2026). The consistent message is a small, tuned graphene share, not a graphene-rich hybrid.

Architecture can substitute for filler. The 3D microflower aerogel reaches −63.2 dB with only 8 wt% filler (Shi et al., 2026). Conventional powders in paraffin commonly use higher loadings, for example 25 wt% in Li et al. (2024). Because areal density is a RAM requirement, filler loading should be a headline metric, not a footnote.

Hybrids can lose to the pure phase. The combustion study (Tayebi Pak et al., 2021) shows pure Fe_3O_4 matching or beating a Fe_3O_4/rGO powder. This finding is rarely repeated in the field and deserves explicit control experiments in any new study.

GO-based work is scarce. Only one 2026 study in this set describes Fe_3O_4-decorated GO as such and links it to RCS values (Huang et al., 2026). The effect of leaving oxygen groups in place on bandwidth and stability remains an open research question.

Once a binary GO/Fe_3O_4 hybrid reaches its ceiling, studies add a third component or reshape the structure. The strategies below recur, and each trades extra complexity for either more loss mechanisms or better matching.

Core–shell and carbon-coated Fe_3O_4. Fe_3O_4@C and Fe_3O_4@polymer cores combined with rGO use the shell to raise permittivity in a controlled way and to separate the magnetic cores. Porous Fe_3O_4@C core/shell nanorods on rGO showed that rGO reduced agglomeration and improved matching and dielectric loss (Fu et al., 2018). Fe_3O_4@PEDOT microspheres on rGO reached −48.8 dB at 2.9 mm with 4.32 GHz EAB and were evaluated by RCS simulation (Chen et al., 2021). Related non-graphene core–shell work includes Fe_3O_4@MnO_2 (Qiao et al., 2016). Similar ideas appear in 3D porous Fe_3O_4/C flowers (Wu et al., 2018a). Fe_3O_4 nanotubes with natural resonance offer a further example (He et al., 2017).

Ternary and heterojunction hybrids. Adding a second loss phase creates more interfaces. Fe_3O_4/$CoCO_3$@rGO covered the entire Ku-band and part of the X-band at 2.1 mm (Li et al., 2024). Fe_3O_4/FeS_x hollow spheres in an rGO aerogel combined a hollow structure and multiple interfaces for −43.03 dB at 2.0 mm (J. Zhang et al., 2024). Fe_3O_4/Fe nanorings on rGO were reported earlier (Ding et al., 2016). Fe_3O_4/Fe heterojunctions on rGO reached −66.4 dB with 7.16 GHz EAB and also gave infrared stealth, hydrophobicity and EMI shielding (Pan et al., 2026). Combinations with MoS_2 and with MXene-type Nb_2CT_x are cited among Fe_3O_4/rGO ternaries, for example Fe_3O_4/MoS_2/rGO with −66.92 dB at 3.61 mm, as reported in Zhang et al. (2024b). Transition-metal dichalcogenides more broadly are reviewed in Cheng et al. (2024).

Polymer partners. PANI/GO/Fe_3O_4 nanocomposites add a conducting-polymer dielectric loss channel (Zhao et al., 2015).

3D and hierarchical structures. 3D graphene–Fe_3O_4 nanocomposites were an early example (Hu et al., 2013). Porous aerogels and microflowers provide continuous conductive and scattering networks at very low filler loading (Shi et al., 2026). Multi-scale design, from atoms to macrostructures, is now reviewed as a general route for graphene-based absorbers (Liu et al., 2026).

Other carbon forms. The Fe_3O_4/nanocarbon buckypaper work reports that Fe_3O_4/GO papers outperform Fe_3O_4/MWCNT papers in minimum reflection loss and effective bandwidth, and that such papers can be applied as a coating on epoxy/fibre composites (Wang et al., 2019). MOF-derived porous carbons offer a related route to tuneable carbon–magnetic hybrids (Zhang et al., 2021).

Assessment. These designs push RL_{min} below −60 dB, but they also introduce new failure points for RAM use: extra processing steps, sulfide or carbonate phases with unknown long-term stability, and larger batch-to-batch scatter. A practical RAM programme will probably prefer a robust binary or simple ternary hybrid with a clear scale-up path over the most elaborate heterostructure.

International Journal of Health Sciences is licensed under a Creative Commons Attribution 4.0 International License

e-ISSN : 2987-0836 DOI: https://doi.org/10.59585/ijhs

Publish : Association of Indonesian Teachers and Lecturers
International Journal of Health Sciences (IJHS)
Journal Homepage : https://jurnal.agdosi.com/index.php/IJHS/index
Volume 4 | Number 4 | December 2026 |

Most GO/Fe_3O_4 papers stop at coaxial-ring data in paraffin. RAM adoption needs evidence at three further levels.

A growing minority of studies simulate RCS for a coated metal plate or a platform model. Examples include Fe_3O_4@PEDOT/rGO on an Al plate (Chen et al., 2021). Covalently bonded rGO–Fe_3O_4 was evaluated in the same way (Liu et al., 2021). So was Fe_3O_4/Fe@rGO (Pan et al., 2026). For Fe_3O_4@GO, the simulated RCS stayed below −16.06 dB m² across −90° to 90°, with a minimum of −29.04 dB m² at 10° (Huang et al., 2026). Related absorber papers use CST models of a drone coating at 10 GHz (Han et al., 2024), which shows the method for a different absorber. These simulations take the measured ε and μ as input, so they confirm the trend of the coupon data but not the real-world coating behaviour. Free-space or arch (NRL) measurements on coated panels are still largely missing.

Integration routes reported so far include epoxy-based composites with heat-reduced rGO/Fe_3O_4 (H.-K. Liu et al., 2023). Fe_3O_4/GO buckypaper layers have been applied to epoxy/fibre laminates (Wang et al., 2019). In silicone rubber, rGO/Fe_3O_4 provides infrared stealth in addition to −31.3 dB at 15.3 GHz (Wu et al., 2022). A flexible Fe_3O_4/Fe@rGO film combined microwave absorption with infrared stealth, hydrophobicity and EMI shielding (Pan et al., 2026). Multilayer and gradient designs, which are recommended to widen the band in the stealth literature (Ahmad et al., 2019), are almost absent for GO/Fe_3O_4 even though the permittivity tuning described in Section 3.3 is well suited to gradient design.

Thermal stability is one of the few service-environment properties reported: an iron oxide/rGO composite made thermochemically was stable up to 800 °C and was proposed for high-temperature absorption (Zhang et al., 2015). Other issues that RAM programmes care about, such as Fe_3O_4 oxidation to γ-Fe_2O_3 or α-Fe_2O_3, humidity, salt fog, UV and thermal cycling, adhesion on metal, and rain erosion, are essentially unreported for these hybrids. Fe_3O_4 is a reasonably stable oxide, but the GO/rGO interface in humid or hot conditions needs data.

Because weight matters on aircraft and ships, the areal density at matching thickness should accompany RL. A paraffin ring containing 25 wt% filler and a 3D aerogel at 8 wt% may have similar RL but very different mass per unit area (Table 6). We recommend reporting RL_{min}, EAB, thickness, filler loading, matrix, density and areal density together so that a reader can compare absorbers on a mass-adjusted basis.

The mainstream explanation of absorber performance, used throughout this field, rests on impedance matching theory and the quarter-wavelength model (Naito & Suetake, 1971). A group of authors argues that these tools are widely misapplied. Their main claims, published in peer-reviewed papers and in preprints, are threefold. First, RL is an innate property only of a metal-backed film and not of the material itself (Y. Liu et al., 2023). Second, impedance matching theory, derived for the scattering parameter S_{11}, cannot be applied to RL (Y. Liu, Drew, et al., 2023). Third, absorption peaks in a metal-backed film arise from wave interference between reflected beams, not from more energy entering the material (Y. Liu et al., 2022). A 2025 article in *Advanced Electronic Materials* on quality criteria for microwave absorbing materials acknowledges that extreme RL values are device-level outcomes and not intrinsic properties (Yang et al., 2025). The critique has also been aimed at perspectives that restate the impedance-matching view (Hou et al., 2024).

This review does not take a side. The practical consequence for GO/Fe_3O_4 studies is modest and easy to follow: (i) describe RL as the performance of a metal-backed layer of stated thickness and not as a material constant; (ii) avoid causal claims from impedance-matching maps alone, and support mechanisms with independent measurements; (iii) cite the framework limitations explicitly

International Journal of Health Sciences is licensed under a Creative Commons Attribution 4.0 International License

e-ISSN : 2987-0836 DOI: https://doi.org/10.59585/ijhs

Publish : Association of Indonesian Teachers and Lecturers
International Journal of Health Sciences (IJHS)
Journal Homepage : https://jurnal.agdosi.com/index.php/IJHS/index
Volume 4 | Number 4 | December 2026 |

so that reviewers see that they were considered. The details of this debate remain unresolved. Table 7 lists practical steps that make reported data comparable.

Table 7. Issues that limit comparison of reported data, with recommended practice.

Issue	Why it matters	Recommended practice
Matrix and loading	Paraffin at 25 wt% and epoxy at 40 wt% give different ε and μ (H.-K. Liu et al., 2023)	State filler wt% and vol%, matrix, density, preparation method
Thickness window	A peak at 6.5 mm and one at 1.6 mm are not equal for RAM (Du et al., 2020)	Report RL at 1–5 mm and the thickness for EAB maximum
Frequency range	Bandwidths in 2–18 GHz may omit the X-band target	Report coverage of X and Ku separately
Carbon state	"GO" in a title may be rGO in the product (Zhang et al., 2015)	Report C/O (XPS), I_D/I_G, XRD (001) position and TGA-based Fe_3O_4 fraction (Section 3.3.3)
Control samples	Pure Fe_3O_4 can outperform a hybrid (Tayebi Pak et al., 2021)	Always include pure Fe_3O_4, GO/rGO and a physical mixture
Repeatability	Single-sample curves hide scatter	Measure at least three samples; report uncertainty
Single metric	RL_{min} alone favours narrow peaks (Yang et al., 2025)	Report RL_{min}, EAB, thickness, areal density together
Simulation claims	RCS depends on assumed geometry	State model, polarization, frequency and the input ε, μ (Huang et al., 2026)

The literature lacks three controls that reviewers will expect in a primary study: a physical Fe_3O_4 + GO mixture to show that chemical bonding or intimate interfaces matter; a GO versus rGO series at fixed Fe_3O_4 content; and a thickness-resolved check of the quarter-wavelength prediction against measured data. These controls are inexpensive and would raise the evidential value of future papers.

4. Conclusion

GO/rGO–Fe_3O_4 hybrids are a credible family of lightweight microwave absorbers. The best systems reach RL_{min} of −43 to −66 dB at 2–3 mm, with 6–7 GHz of EAB in the Ku-band, mainly through a tuned graphene fraction, abundant Fe_3O_4/carbon heterointerfaces and porous or hierarchical structures. Three limitations hold the field back from RAM use. First, most reports use rGO, so the benefit of GO's oxygen groups is largely untested. Second, hybrids do not always beat pure Fe_3O_4, and control experiments are needed to show where synergy exists. Third, evidence stops at paraffin or epoxy coupons, with limited RCS simulation, almost no free-space data and very little durability data. Studies that add GO-versus-rGO series, physical-mixture controls, mass-adjusted metrics and coating-scale validation, and that frame RL carefully, would give the field the evidence that RAM developers need.

5. Compliance with ethical standards

Acknowledgements

This research received no external funding

Disclosure of conflict of interest

The authors declare no known competing financial interests or personal relationships that could have influenced this work.

Statement of informed consent

Not applicable. This review is based on published literature and did not involve human participants.

International Journal of Health Sciences is licensed under a Creative Commons Attribution 4.0 International License

e-ISSN : 2987-0836 DOI: https://doi.org/10.59585/ijhs

Publish : Association of Indonesian Teachers and Lecturers
International Journal of Health Sciences (IJHS)
Journal Homepage : https://jurnal.agdosi.com/index.php/IJHS/index
Volume 4 | Number 4 | December 2026 |

Author contributions (CRediT)

Conceptualization; Methodology; Investigation; Writing – original draft; Writing – review & editing.

Data availability

No new data were generated. All values are taken from the cited publications; the literature-search records are available on request.

Declaration of generative AI use

During the preparation of this manuscript, the author(s) used Claude (Anthropic) to assist with drafting, language editing and reference formatting. The author(s) reviewed and edited all content and take full responsibility for the published work

References

Adebayo, L. L., et al. (2020). Recent advances in the development of Fe_3O_4-based microwave absorbing materials. *Ceramics International*, *46*(2), 1249–1268. https://doi.org/10.1016/j.ceramint.2019.09.209

Ahmad, H., et al. (2019). Stealth technology: Methods and composite materials—a review. *Polymer Composites*. https://doi.org/10.1002/pc.25311

Chen, X., et al. (2021). Enhanced electromagnetic wave absorption performance of core-shell Fe_3O_4@poly(3,4-ethylenedioxythiophene) microspheres/reduced graphene oxide composite. *Carbon*, *178*, 273–284.

Cheng, J., et al. (2021). Construction of multiple interfaces and dielectric/magnetic heterostructures in electromagnetic wave absorbers with enhanced absorption performance: A review. *Journal of Materiomics*, *7*(6), 1233–1263. https://doi.org/10.1016/j.jmat.2021.02.017

Cheng, J., et al. (2024). From VIB- to VB-group transition metal disulfides: Structure engineering modulation for superior electromagnetic wave absorption. *Nano-Micro Letters*, *16*, Article 29. https://doi.org/10.1007/s40820-023-01247-7

Compton, O. C., et al. (2011). Chemically active reduced graphene oxide with tunable C/O ratios. *ACS Nano*, *5*, 4380–4391.

Dimiev, A. M., Alemany, L. B., & Tour, J. M. (2013). Graphene oxide. Origin of acidity, its instability in water, and a new dynamic structural model. *ACS Nano*, *7*, 576–588.

Dimiev, A. M., & Tour, J. M. (2014). Mechanism of graphene oxide formation. *ACS Nano*, *8*, 3060–3068.

Ding, Y., et al. (2016). Electromagnetic wave absorption in reduced graphene oxide functionalized with Fe_3O_4/Fe nanorings. *Nano Research*, *9*, 2018–2025.

Du, Z., et al. (2020). One-pot hydrothermal preparation of Fe_3O_4 decorated graphene for microwave absorption. *Materials*, *13*(14), Article 3065. https://doi.org/10.3390/ma13143065

Edries, M., et al. (n.d.). Radar-absorbing materials, metamaterials, and metasurfaces: Design methods, considerations, and best practices. In *Advances and applications of metamaterials and metasurfaces through RF to optic spectrum*. IntechOpen. https://doi.org/10.5772/intechopen.1014249

Fu, C., et al. (2018). Facile synthesis of porous Fe_3O_4@C core/shell nanorod/graphene for improving microwave absorption properties. *RSC Advances*, *8*(28), 15358–15365. https://doi.org/10.1039/C8RA01838C

Gu, F., Jin, S., Tang, S., et al. (2019). Comparative study of deoxygenation behavior for graphene oxide with different oxidation degree and mildly reduced graphene oxide via solid-state microwave irradiation. *Materials Chemistry and Physics*.

Han, Y., Chen, F., & Fu, Q. (2024). Heterogeneous three-dimensional FeSiAl@SiO_2@MoS_2 composite with a SiO_2 wave-transmitting layer for enhanced electromagnetic wave absorption performance. *Journal of Materials Chemistry A*. https://doi.org/10.1039/D4TA04820B

He et al. (2017). Lightweight ferroferric oxide nanotubes with natural resonance property and design for broadband microwave absorption. *Journal of Materials Science*, *52*, 8258.

Hou et al. (2024). A perspective on impedance matching and resonance absorption mechanism for electromagnetic wave absorbing. *Carbon*, *222*, Article 118935.

Houbi, A., et al. (2021). Microwave absorbing properties of ferrites and their composites: A review. *Journal of Magnetism and Magnetic Materials*, *529*, Article 167839.

Hu, C., et al. (2013). 3D graphene–Fe_3O_4 nanocomposites with high-performance microwave absorption. *Physical Chemistry Chemical Physics*, *15*(31), 13038–13043. https://doi.org/10.1039/C3CP51253C

International Journal of Health Sciences is licensed under a Creative Commons Attribution 4.0 International License

e-ISSN : 2987-0836 DOI: https://doi.org/10.59585/ijhs

Publish : Association of Indonesian Teachers and Lecturers
International Journal of Health Sciences (IJHS)
Journal Homepage : https://jurnal.agdosi.com/index.php/IJHS/index
Volume 4 | Number 4 | December 2026 |

Huang, X., et al. (2026). Magneto-dielectric synergy: One-pot synthesis of Fe_3O_4 nanoparticle-decorated graphene oxide for high performance electromagnetic wave absorption. *Journal of Materials Chemistry C*. https://doi.org/10.1039/D6TC00669H

Hummers, W. S., & Offeman, R. E. (1958). Preparation of graphitic oxide. *Journal of the American Chemical Society*, *80*, 1339.

Jian, X., et al. (2016). Facile synthesis of Fe_3O_4/GCs composites and their enhanced microwave absorption properties. *ACS Applied Materials & Interfaces*, *8*, 6101. https://doi.org/10.1021/acsami.6b00388

Jiao, S., et al. (2020). Enhanced microwave absorption: The composite of Fe_3O_4 flakes and reduced graphene oxide with improved interfacial polarization. *Advanced Engineering Materials*, *22*(4), Article 1901299. https://doi.org/10.1002/adem.201901299

Kim, S.-H., et al. (2023). Carbon-based radar absorbing materials toward stealth technologies. *Advanced Science*, *10*(32), Article 2303104. https://doi.org/10.1002/advs.202303104

Lerf, A., et al. (1998). Structure of graphite oxide revisited. *Journal of Physical Chemistry B*, *102*, 4477–4482.

Li, H., et al. (2024). Facile synthesis of Fe_3O_4/$CoCO_3$ nanoparticles anchored on reduced graphene oxide for highly efficient microwave absorption. *Journal of Materials Science: Materials in Electronics*. https://doi.org/10.1007/s10854-024-12734-x

Li, J.-S., et al. (2017). Research progress of graphene-based microwave absorbing materials in the last decade. *Journal of Materials Research*, *32*(7), 1213–1230. https://doi.org/10.1557/jmr.2017.80

Liu, H.-K., Yang, R.-B., & Wu, Y. S. (2023). Microwave absorbing properties of heat reduced graphene oxide/Fe_3O_4/epoxy hybrid composites. In *Proceedings of the 23rd International Conference on Composite Materials (ICCM23)*.

Liu, J., et al. (2022). Progress in preparation, characterization, surface functional modification of graphene oxide: A review. *Journal of Saudi Chemical Society*, *26*, Article 101560. https://doi.org/10.1016/j.jscs.2022.101560

Liu, X., et al. (2021). Synthesis of covalently bonded reduced graphene oxide-Fe_3O_4 nanocomposites for efficient electromagnetic wave absorption. *Journal of Materials Science & Technology*, *72*, 93–103. https://doi.org/10.1016/j.jmst.2020.09.012

Liu, Y., Drew, M. G. B., & Liu, Y. (2023). A physics investigation on impedance matching theory in microwave absorption film—Part 1: Theory. *Journal of Applied Physics*, *134*(4), Article 045303. https://doi.org/10.1063/5.0153608

Liu, Y., Liu, Y., & Drew, M. G. B. (2022). A re-evaluation of the mechanism of microwave absorption in film—Part 1: Energy conservation. *Materials Chemistry and Physics*.

Liu, Y., et al. (2023). Unexpected results in microwave absorption—Part 1: Different absorption mechanisms for metal-backed film and for material. *Surfaces and Interfaces*, *40*, Article 103022.

Liu, Z., Chen, X.-B., & Yue, H. (2026). From atoms to macrostructures: Multiscale design and evolution of graphene-based electromagnetic wave absorbing materials. *Nano Research*. https://doi.org/10.26599/NR.2026.94909154

Marcano, D. C., Kosynkin, D. V., Berlin, J. M., et al. (2010). Improved synthesis of graphene oxide. *ACS Nano*, *4*, 4806–4814.

Massart, R. (1981). Preparation of aqueous magnetic liquids in alkaline and acidic media. *IEEE Transactions on Magnetics*, *17*, 1247–1248.

Meng, F., et al. (2018). Graphene-based microwave absorbing composites: A review and prospective. *Composites Part B: Engineering*, *137*, 260–277. https://doi.org/10.1016/j.compositesb.2017.11.023

Naito, Y., & Suetake, K. (1971). Application of ferrite to electromagnetic wave absorber and its characteristics. *IEEE Transactions on Microwave Theory and Techniques*, *19*, 65–72.

Nurhasmi. (2026). Effect of cavity-based surface geometry on electromagnetic wave absorption in radar absorbing materials: A review. *Pinisi Physics Journal*, *2*(1).

Oh, J.-H., et al. (2004). Design of radar absorbing structures using glass/epoxy composite containing carbon black in X-band frequency ranges. *Composites Part B: Engineering*, *35*(1), 49.

Pan, Y., et al. (2026). Fe-based multi-interfacial engineering composites for broadband electromagnetic wave absorption. *Nano Research*, Article 94908326. https://doi.org/10.26599/NR.2026.94908326

Pei, S., & Cheng, H.-M. (2012). The reduction of graphene oxide. *Carbon*, *50*, 3210–3228.

Peng, F., et al. (2022). Progress in graphene-based magnetic hybrids towards highly efficiency for microwave absorption. *Journal of Materials Science & Technology*, *106*, 147–161. https://doi.org/10.1016/j.jmst.2021.06.066

Peng, L., Xu, Z., Liu, Z., et al. (2015). An iron-based green approach to 1-h production of single-layer graphene oxide. *Nature Communications*, *6*, Article 5716.

Qiao et al. (2016). Dependency of tunable microwave absorption performance on morphology-controlled hierarchical shells for core-shell Fe_3O_4@MnO_2 composite microspheres. *Chemical Engineering Journal*, *304*, 552.

Qin, M., Zhang, L., & Wu, H. (2022). Dielectric loss mechanism in electromagnetic wave absorbing materials. *Advanced Science*, *9*(10), Article 2105553. https://doi.org/10.1002/advs.202105553

International Journal of Health Sciences is licensed under a Creative Commons Attribution 4.0 International License

Publish : Association of Indonesian Teachers and Lecturers
International Journal of Health Sciences (IJHS)
Journal Homepage : https://jurnal.agdosi.com/index.php/IJHS/index
Volume 4 | Number 4 | December 2026 |

Quan, B., et al. (2017). Dielectric polarization in electromagnetic wave absorption: Review and perspective. *Journal of Alloys and Compounds*, *728*, 1065.

Ren, J., Zhang, L., & Fan, X. (2021). Rational self-assembly of Fe_3O_4 nanostructures on reduced graphene oxide for enhanced microwave absorption. *Journal of Electronic Materials*, *50*(9), 5057–5071. https://doi.org/10.1007/s11664-021-09013-4

Rourke, J. P., Pandey, P. A., Moore, J. J., et al. (2011). The real graphene oxide revealed: Stripping the oxidative debris from the graphene-like sheets. *Angewandte Chemie International Edition*, *50*, 3173–3177.

Ruiz-Perez, F., et al. (2022). Carbon-based radar absorbing materials: A critical review. *Journal of Science: Advanced Materials and Devices*.

Saville, P. (2005). *Review of radar absorbing materials* (DRDC Atlantic TM 2005-003). Defence R&D Canada – Atlantic.

Shi, S., et al. (2026). Rational design of lightweight microwave absorbers: Synergistic dielectric–magnetic loss in 3D hierarchical graphene/Fe_3O_4 microflower composites. *Journal of Materials Chemistry C*. https://doi.org/10.1039/D6TC01516F

Snoek, J. L. (1948). Dispersion and absorption in magnetic ferrites at frequencies above one Mc/s. *Physica*, *14*, 207–217.

Stankovich, S., Dikin, D. A., Dommett, G. H. B., et al. (2006). Graphene-based composite materials. *Nature*, *442*, 282–286.

Sun, X., He, J., Li, G., et al. (2013). Laminated magnetic graphene with enhanced electromagnetic wave absorption properties. *Journal of Materials Chemistry C*, *1*, 765–777.

Tang, L., Li, X., Ji, R., et al. (2012). Bottom-up synthesis of large-scale graphene oxide nanosheets. *Journal of Materials Chemistry*, *22*, 5676–5683.

Tayebi Pak, A., et al. (2021). Hierarchical porous Fe_3O_4/RGO nanocomposite powders as high performance microwave absorbers. *Journal of Materials Research and Technology*, *13*, 548–560.

Trikkaliotis, D. G., et al. (2021). Graphene oxide synthesis, properties and characterization techniques: A comprehensive review. *ChemEngineering*, *5*, Article 64. https://doi.org/10.3390/chemengineering5030064

Wang, J., et al. (2019). Preparation and microwave absorption performance of a flexible Fe_3O_4/nanocarbon hybrid buckypaper and its application in composite materials. *RSC Advances*, *9*, 37870. https://doi.org/10.1039/C9RA07406F

Wen, B., Cao, M., et al. (2014). Reduced graphene oxides: Light-weight and high-efficiency electromagnetic interference shielding at elevated temperatures. *Advanced Materials*, *26*, 3484–3489.

Wu et al. (2018a). Enhanced electromagnetic wave absorption of three-dimensional porous Fe_3O_4/C composite flowers. *ACS Sustainable Chemistry & Engineering*, *6*, 12471.

Wu, F., et al. (2018b). The effects of annealing temperature on the permittivity and electromagnetic attenuation performance of reduced graphene oxide. *Applied Physics Letters*, *112*(19), Article 192902. https://doi.org/10.1063/1.5028472

Wu, J., et al. (2017). The effect of GO loading on electromagnetic wave absorption properties of Fe_3O_4/reduced graphene oxide hybrids. *Ceramics International*, *43*, 13146–13153.

Wu, K.-H., et al. (2022). Infrared stealth and microwave absorption properties of reduced graphene oxide functionalized with Fe_3O_4. *Materials Science and Engineering: B*, *276*, Article 115575.

Xia, Y., et al. (2018). Controlled hydrothermal temperature provides tunable permittivity and an improved electromagnetic absorption performance of reduced graphene oxide. *RSC Advances*, *8*, 33065–33071. https://doi.org/10.1039/C8RA05843A

Yang, S., et al. (2025). On the quality criteria for microwave absorbing materials. *Advanced Electronic Materials*, *11*(14), Article e00239. https://doi.org/10.1002/aelm.202500239

Yu, Q., et al. (2019). Reduced graphene oxide-wrapped super dense Fe_3O_4 nanoparticles with enhanced electromagnetic wave absorption properties. *Nanomaterials*, *9*(6), Article 845. https://doi.org/10.3390/nano9060845

Zhang, J., et al. (2024). Fe_3O_4/FeS_x hollow heteronanospheres/reduced graphene oxide aerogel for electromagnetic wave absorption. *Materials Research Bulletin*.

Zhang, K., et al. (2024). Dielectric–magnetic manipulation of reduced graphene oxide permittivity for enhanced electromagnetic wave absorption. *Journal of Advanced Ceramics*. https://doi.org/10.26599/JAC.2024.9220990

Zhang, L., et al. (2015). Facile synthesis of iron oxides/reduced graphene oxide composites: Application for electromagnetic wave absorption at high temperature. *Scientific Reports*, *5*, Article 9298. https://doi.org/10.1038/srep09298

Zhang, R., et al. (2016). Enhanced microwave absorption properties of ferroferric oxide/graphene composites with a controllable microstructure. *RSC Advances*, *6*, 16952–16962.

Zhang, Z., et al. (2021). A review on metal–organic framework derived porous carbon-based novel microwave absorption materials. *Nano-Micro Letters*, *13*, Article 56. https://doi.org/10.1007/s40820-020-00582-3

International Journal of Health Sciences is licensed under a Creative Commons Attribution 4.0 International License

e-ISSN : 2987-0836 DOI: https://doi.org/10.59585/ijhs

Publish : Association of Indonesian Teachers and Lecturers
International Journal of Health Sciences (IJHS)
Journal Homepage : https://jurnal.agdosi.com/index.php/IJHS/index
Volume 4 | Number 4 | December 2026 |

Zhao, J., et al. (2015). Synthesis and electromagnetic, microwave absorbing properties of polyaniline/graphene oxide/Fe_3O_4 nanocomposites. *RSC Advances*, *5*, 19345–19352.

Zhao, X., et al. (2013). Excellent microwave absorption property of graphene-coated Fe nanocomposites. *Scientific Reports*, *3*, Article 3421.

Zhou, M., Zhou, Z., & Cheng, H. (2026). Composition and structural design of magnetic alloy/composites for high-performance microwave absorption: A review. *Nanomaterials*, *16*(5), Article 290. https://doi.org/10.3390/nano16050290

International Journal of Health Sciences is licensed under a Creative Commons Attribution 4.0 International License